Original article

Synthesis of coumarin derivatives as fluorescent probes for membrane and cell dynamics studies

Olimpo García-Beltrán [a,b,*], Osvaldo Yañez [c], Julio Caballero [c], Antonio Galdámez [a], Natalia Mena [d], Marco T. Nuñez [d], Bruce K. Cassels [a]

[a] Department of Chemistry, Faculty of Sciences, University of Chile, Santiago, Chile
[b] Facultad de Ciencias Naturales y Matemáticas, Universidad de Ibagué, Carrera 22 Calle 67, Ibagué, Colombia
[c] Centro de Bioinformática y Simulación Molecular, Facultad de Ingeniería, Universidad de Talca, 2 Norte 685, Casilla 721, Talca, Chile
[d] Department of Biology, Faculty of Sciences, University of Chile, Santiago, Chile

ABSTRACT

Three coumarin-derived fluorescent probes, 3-acetyl-7-[(6-bromohexyl)oxy]-2H-chromen-2-one (**FM1**), 7-[(6-bromohexyl)oxy]-4-methyl-2H-chromen-2-one (**FM2**) and ethyl 2-{7-[(6-bromohexyl)oxy]-2-oxo-2H-chromen-4-yl}acetate (**FM3**), are described, with their photophysical constants. The compounds were tested in preliminary studies employing epifluorescence microscopy demonstrating that they allow the imaging of human neuroblastoma SH-SY5Y cell membranes. The structure of **FM3** was confirmed by X-ray crystallographic analysis. Molecular dynamics (MD) simulations were used to characterize the localization and interactions of the studied compounds with a lipid bilayer model of 1-palmitoyl-2-oleoyl-sn-glycero-3-phosphocholine (POPC).

1. Introduction

A biomembrane is a dynamic structure that acts as the primary barrier isolating the cell cytosol from the extracellular medium or separating distinct cell compartments [1]. Its fundamental structure is a phospholipid bilayer presenting at least two distinct chemical regions, a hydrophobic region inside the membrane and a hydrophilic region distributed between the interfaces with the cytosol and the cell exterior or the interior of specific intracellular structures [2]. A main function of biological membranes is to ensure the integrity of the cell itself or of certain organelles, and to control the functions of membrane proteins [3—6]. Cell membranes are critical for communication with the outer world by enabling the transfer of many compounds important for cell metabolism and for chemical and electrical signaling [7]. This function requires the correct assembly of various molecular structures in and around the cell membrane including receptors, transport proteins and specialized membranes [8]. For many years lipids were viewed as randomly organized building blocks of biological membranes. This interpretation was adopted from the Singer and Nicholson fluid mosaic model, proposed in 1972 [9]. However, in the 1990s, this was gradually superseded by the raft hypothesis, which proposed a laterally segregated distribution of lipid molecules [10—12]. Information on structures and processes occurring at different depths in a membrane has been obtained using fluorescent or photoactive probes. Both techniques are based on the fact that the membrane hydrophobic core incorporates nonpolar lipid fatty acyl chains, and a fluorescent or photoactive chromophore can be attached to the nonpolar moieties to increase its affinity for the core region [13]. Numerous fluorescent probes have been used that partition into the membrane hydrophobic region, e.g. diphenylhexatriene and anilinonapthalene sulfonic acid. However, the use of such probes only provides average information on the nature of the membrane. In order to get depth-dependent information, a practical approach has been to attach such fluorescent probes to fatty acids at distinct positions so that the membranes can be probed at different depths [14,15]. Fluorescence microscopy is widely used for studying the organization and dynamics of membranes [16,17]. The advantages of this technique include high sensitivity and time resolution, multiple measurable parameters yielding complementary information, and spatial resolution. However, the use of fluorescent probes in membrane studies can potentially cause significant perturbations in membrane

* Corresponding author. Facultad de Ciencias Naturales y Matemáticas, Universidad de Ibagué, Carrera 22 Calle 67, Ibagué, Colombia.
E-mail addresses: ojgarciab@ug.uchile.cl, ojgarciab@yahoo.com (O. García-Beltrán).

structure, dynamics and thermotropic behavior [18–22]. Molecular dynamics (MD) simulations, by providing detailed atomic-scale information on phospholipid bilayers [23,24], represent a valuable complement to these studies by detecting and quantifying the magnitude of the perturbations induced by molecular probes in the host lipid structure.

We have now shown that three new coumarin-derived fluorescent probes are useful to image the plasmalemma of cultured human neuroblastoma cells, and obtained a more detailed picture of this finding by determining the crystal structure of one of these probes and characterizing the localization and interactions of the studied compounds with a lipid bilayer model by MD simulations.

2. Results and discussion

Chemistry. Fluorescent probes **FM1**, **FM2** and **FM3** were designed to provide appropriate lipophilicity while also allowing for further derivatization by substitution of the terminal bromine atom. The route employed is summarized in Scheme 1 (Supporting Information). The compounds were obtained starting from resorcinol, which was formylated using the Vilsmeier–Haack reaction [37]. Knoevenagel condensation of the aldehyde intermediate (**1**) with ethyl acetoacetate afforded hydroxycoumarin **2** [25], while compound **3** was synthesized through Pechmann condensation of **1** with citric acid and was subsequently esterified to obtain compound **4** [26]. Reaction of 7-hydroxycoumarins **2**, **3** and **4**, in a Williamson-type reaction with 1,6-dibromohexane, gave the corresponding ethers **FM1**, **FM2** and **FM3** [38]. Unexpectedly, the formation of **FM2** was attended by decarboxylation of coumarin **2** in the presence of potassium carbonate, giving the 4-methylcoumarin. Scheme 2 (Supporting Information) shows a possible mechanism for the K-catalyzed protiodecarboxylation. Similar mechanisms have been reported using the decarboxylating agent $AgCO_3$ [39–42], but the present result suggests that expensive silver salts are not necessary to effect this reaction.

Perspective views of the crystal structure of ethyl 2-(7-(6-bromohexyloxy)-2-oxo-2H-chromen-4-yl)acetate (**FM3**) with its atom labels are depicted in Fig. 1. The crystal data, data collection and refinement are summarized in Table 1.
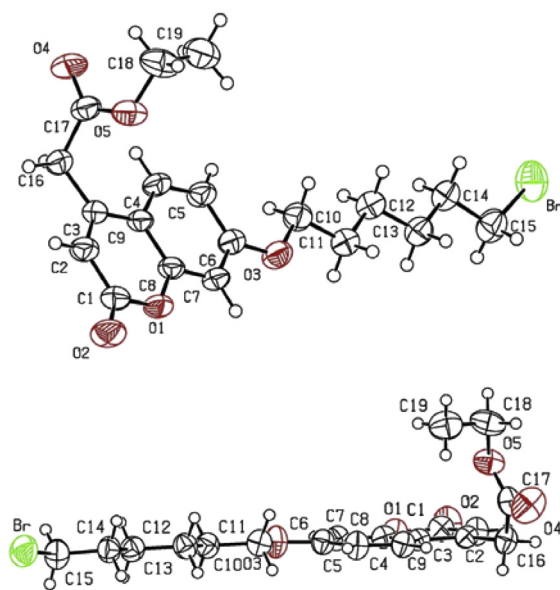
Table 1
Crystal data and details of the structure determination for **FM3**.

Compound	$C_{19}H_{23}O_5Br$
Formula weight	411.28
Crystal shape/color	Block/colorless
Crystal size (mm)	$0.10 \times 0.12 \times 0.30$
Crystal system/space group	Triclinic/P-1
a (Å)	7.7862 (13)
b (Å)	10.2539 (16)
c (Å)	12.105 (3)
α (°)	87.963 (18)
β (°)	77.255 (18)
δ (°)	85.625 (18)
V (Å^3)	939.7 (3)
Z	2
Dcalc (g/cm^{-3})	1.454
Wavelength, Mo Kα (Å)	0.71073
T (K)	293 (2)
F (000)	424
θ-range (°)	$1.73 < \theta < 25.00$
hkl-range	$-8:9, -8:12, -14:14$
μ (mm^{-1})	2.212
Reflections collected/R_{int}/R_σ	7225/0.0209/0.0289
Reflections unique/parameters	2499/231
R, $wR2$ [$F^2 > 2\sigma(F^2)$]	0.0337, 0.0757
R, $wR2$ (all reflections)	0.0501, 0.0838
Goodness-of-Fit on F^2 (GooF = S)	1.025
Residual electron density $\Delta\rho_{max}/\Delta\rho_{min}$ (e Å^{-3})	0.421/−0.428

In **FM3**, the coumarin ring and the aliphatic chain at C6 (the 6-bromohexyloxy substituent) are practically coplanar, with a C10–O3–C6–C5 torsion angle value of 3.1(4)° (Fig. 1). The hexyloxy chain (O3/C10–C15) is essentially flat with average mean deviation of 0.0110 Å from the least-squares plane (where the maximum deviation from the plane is −0.0205 Å for C15). The halogen atom lies in the mean plane of the zigzagging aliphatic chain [C13–C14–C15–Br = −176.00(18)°], while in 7-((6-bromohexyl)oxy)-4-methyl-2-oxo-2H-chromene the bromine atom departs strongly from this plane, with C13–C14–C15–Br = 65.5(4)° [43]. The ethyl acetate substituent group (at C3) in **FM3** is strongly tilted out of the mean plane of the coumarin ring (Fig. 1, bottom), with a C7–C16–C3 angle of 115.9(2)° [C2–C3–C16–C17 = 115.1(3)°]. All the other relevant structural parameters (bond distances and angles) are as expected and in acceptable agreement with the recently described analogues [43–47].

The intermolecular contacts are responsible for the three-dimensional architecture in the crystal packing of **FM3** [48–50]. The antiparallel stacked molecules have π–π interactions with a Cg1···Cg1′ distance of 3.6811(16) Å (Fig. S1; Supporting Information, top). The intermolecular C4–H4···O4 interactions lead to the formation of dimers parallel to [001], which can be described as a graph-set descriptor $R_2^2(14)$ ring (Fig. S1; Supporting Information, bottom). The H···O contact distance is 2.50(2) Å [>D–H···A = 127.5(19)°] and the C···O contact distance is 3.171(3) Å.

Spectral characteristics of **FM1**, **FM2** and **FM3** such as the absorption maxima (λ_{ab}), emission maxima (λ_{em}), molar extinction coefficient (ε), and quantum yield (Φ), were measured in a mixture of ACN and aqueous 20 mM HEPES buffer, pH 7.4, 1:1. Complete data are presented in Table 2. The electronic absorption spectra of probes **FM1** − **FM3** displayed absorption maxima in the region

Fig. 1. Mutually approximately perpendicular views of the structure of **FM3** showing the atom numbering scheme. Displacement ellipsoids are drawn at the 50% probability level and H atoms are shown as small spheres of arbitrary radii.

Table 2
Photochemical properties of **FM1**, **FM2** and **FM3**.

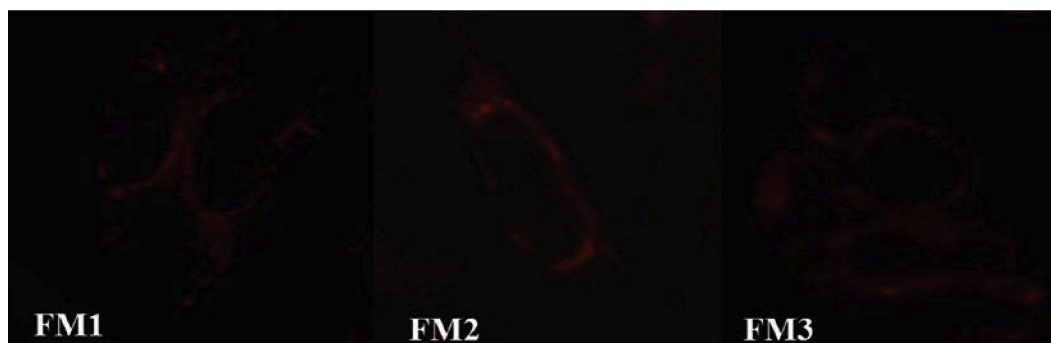| Compounds	λ_{ab} (nm)	λ_{em} (nm)	ε Mol^{-1} dm^{-3} cm^{-1}	Φ	Stokes shift
FM1	360	420	19,786	0.0041	3739
FM2	320	375	13,875	0.259	4584
FM3	310	460	17,703	0.0095	10,819

Fig. 2. SH-SY5Y cells were treated with each compound (**FM1**, **FM2** and **FM3**, 5 μM) for 20 min, after which the fluorescence was measured by epifluorescence microscopy, 63×.

from 300 to 400 nm depending on the nature of the substituent group at C3 or C4 of the coumarin. These absorption bands can be attributed to the benzenoid transition [51]. Regularly, coumarins have been reported to have band groups of UV absorptions at 270–350 nm, due to $\pi-\pi^*$ transitions [52]. A more detailed report shows two band groups at 274–287 and 322–347 nm, with the latter expected to be the result of the overlap of the $\pi-\pi^*$ band with an $n-\pi^*$ band [53]. Comparison of the absorption bands of **FM1**, **FM2** and **FM3** shows a bathochromic shift in **FM1** due to the presence of the carbonyl group at C-3, conjugated with the pyranone ring.

These coumarins exhibit polarity-dependent fluorescence: replacing the 7-OH group of **2**, **3** and **4** with an alkoxy group, their fluorescence intensity increases with increasing polarity of the medium, but with little spectral shift [54,55]. However, the presence of a heavy atom such as bromine on the alkyl chain had not been tested. Although the intensity of the fluorescence spectra of
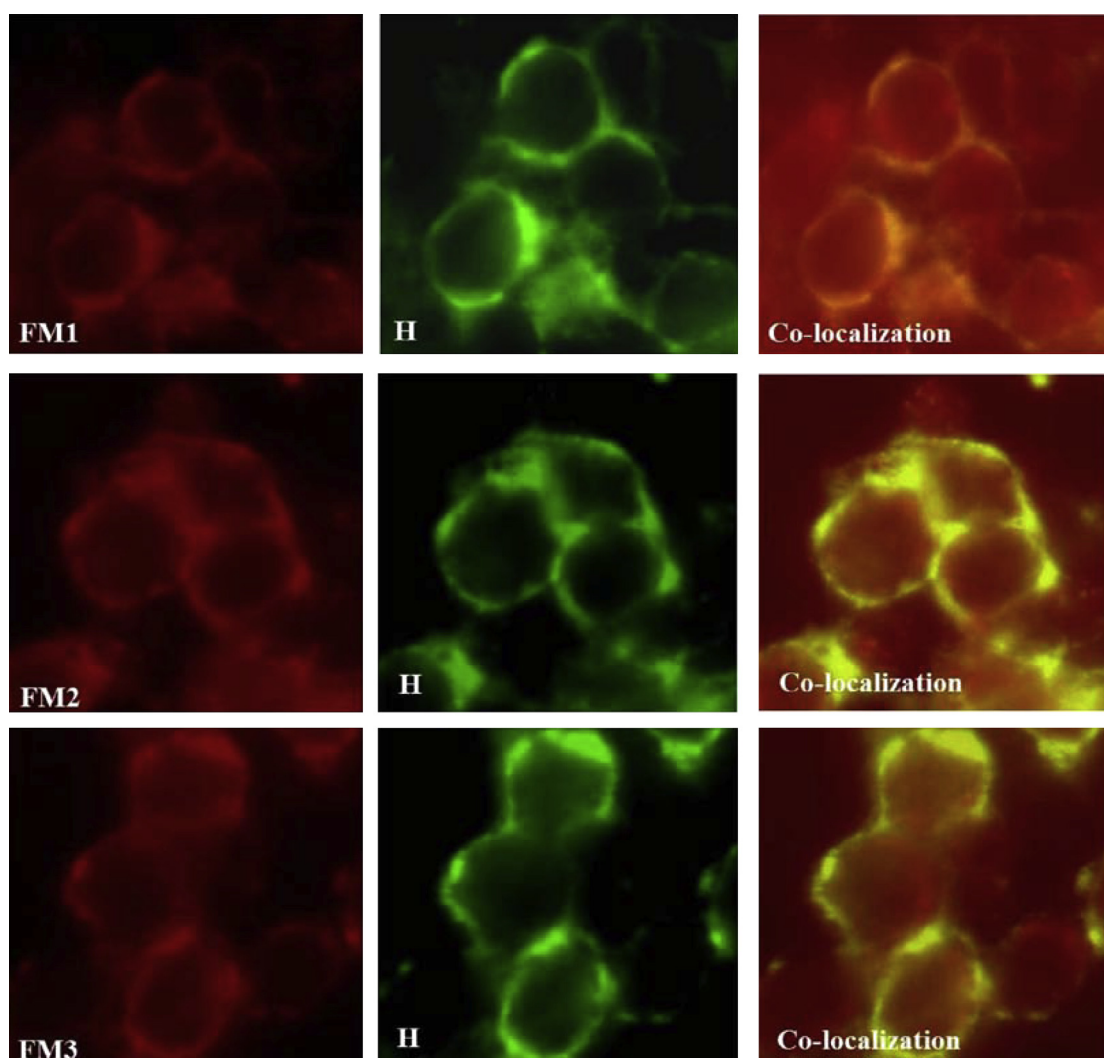

Fig. 3. Cells were incubated for 20 min with 5 μM **FM1**–**FM3** and 5 μM H, and then the fluorescence was recorded by epifluorescence microscopy, 63× objective. Red: **FM1**–**FM3**. Green: H. Yellow: co-localization. (For interpretation of the references to color in this figure legend, the reader is referred to the web version of this article.)

FM1, **FM2** and **FM3** was decreased, the heavy atom effect was unremarkable, especially for compounds **FM2** and **FM3**.

Fluorescence imaging. Knowing the fluorescence behavior of **FM1**–**FM3** in aqueous medium, and considering bibliographic reports on other fluorescent compounds [22,56] with alkyl chains that lead to different localizations in membranes, we proceeded to test their position in the cell membrane of living cells. These experiments were done in SH-SY5Y human neuroblastoma cells. After incubating the cells with each compound, we observed them by epifluorescence microscopy, noting the increased fluorescence intensity caused by accumulation of the coumarins in the periphery of the cells (Fig. 2).

To confirm that the tested compounds were retained in the cell membrane, SH-SY5Y cells were incubated additionally with compound H (unpublished results), a fluorescent membrane probe based on 7-aminocoumarin. This compound has an emission band beyond 500 nm, optimal for a co-localization study. This experiment was followed by epifluorescence microscopy, observing the change in fluorescence caused by the different treatments. The fluorescence due to **FM1**–**FM3** (red) was concentrated in the periphery of the cells, as with H (green) (Fig. 3). The co-localization experiments resulted in emission of yellow light, showing the simultaneous presence of both compounds in the plasma membrane (Fig. 3). Although the test compounds showed a strong preference for the membrane, a weaker red emission was also observed from the cell interior. Compounds **FM2** and **FM3** are better membrane labels than **FM1**, a fact that can be correlated with

their higher quantum yields and solubility in aqueous medium. Considering literature reports [56,57], it seemed likely that the fluorophore of these compounds is outwardly oriented, and the ω-bromoalkyl chains are immersed in the lipid bilayer.

Molecular dynamics. MD simulations of **FM1**–**FM3** in a 1-palmitoyl-2-oleoyl-sn-glycero-3-phosphocholine (POPC) bilayer were performed in order to study the incorporation of the probes into the lipid phase. According to the previous fluorescence measurements, it is expected that these molecules can easily be incorporated into lipid membranes [58]. The studied molecules were initially placed in the bulk water, far from the POPC membrane. **FM1**–**FM3** were incorporated into the membrane and remained within the lipid bilayer for the rest of the simulation time (4.7, 11.6, and 6.9 ns of simulation, respectively) (Fig. 4). This process corresponds to the passive diffusion of the compounds towards the membrane surface. After their incorporation into the membrane, the polar ends of the molecules (oxygens of the 2H-chromen-2-one scaffold) were positioned at the glycerol level of the lipid bilayer with the hydrocarbon chains extended, as in the crystal structure, and located close to the lipid alkyl chains.

There are some differences between the modeled systems due to the different nature of the compounds and their interactions with the membrane. These differences can be easily observed by analysis of the positions of the bromine atoms of the compounds. The presence of the bromine atom close to the center of the membrane indicates that the (6-bromohexyl)oxy group is arranged parallel to the hydrocarbon chains of the lipid bilayer. According to
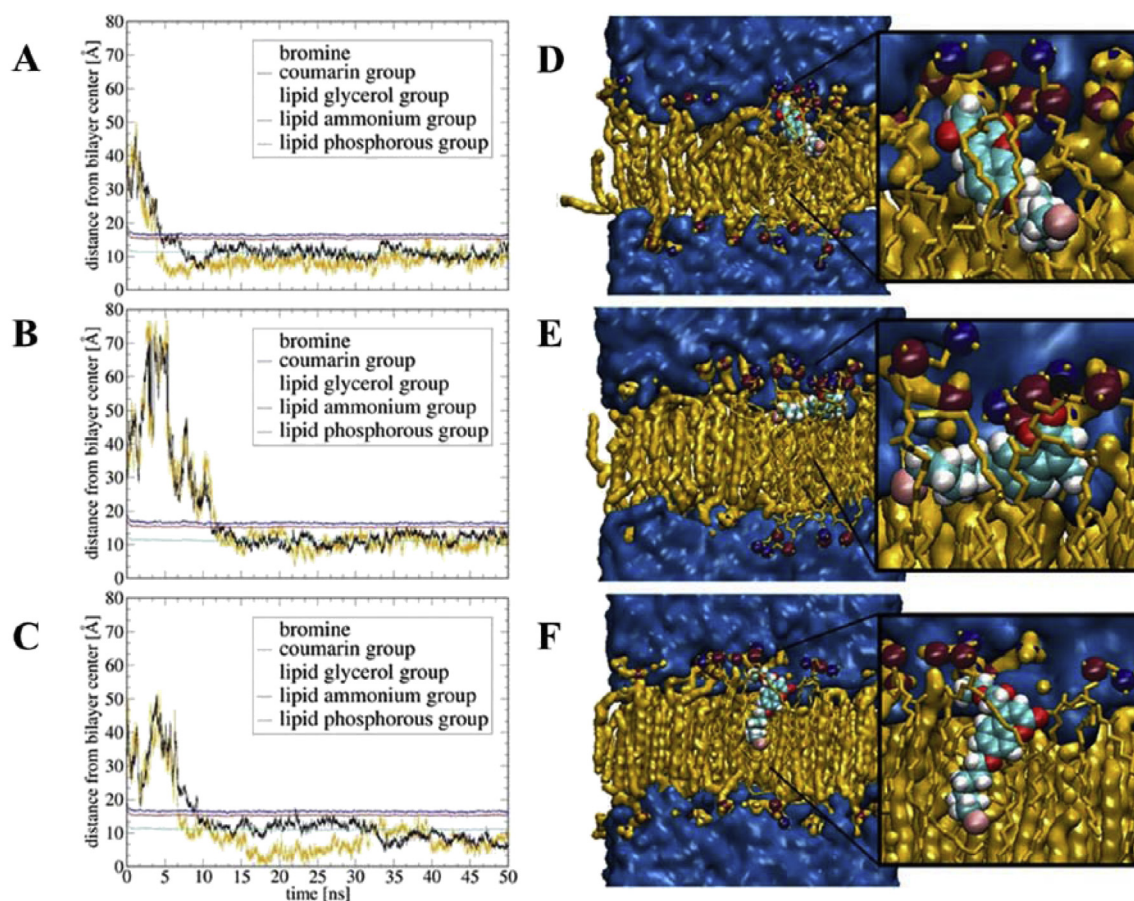

Fig. 4. The dependence of the 2H-chromen-2-one and bromine positions as a function of time of unconstrained MD simulation. (Left) Plots obtained for **FM1** (A), **FM2** (B), and **FM3** (C). Locations of the 2H-chromen-2-one and bromine are depicted by black and orange curves, respectively. The positions of the ammonium (blue curves), phosphorus (red curves) and glycerol (cyan curves) moieties of the lipid are also plotted. (Right) Typical snapshot of a POPC bilayer containing **FM1** (D), **FM2** (E), and **FM3** (F) from MD simulations. Zoomed snapshots are also shown. (For interpretation of the references to color in this figure legend, the reader is referred to the web version of this article.)

this analysis, the positions of **FM1** and **FM3** are better defined than that of **FM2**, which shows a slower stabilization with major fluctuations (Fig. 4), indicating a greater mobility of this compound within the membrane. The bromine atom of **FM1** plunges into the membrane at 5 ns simulation, and the same happens with the **FM3** bromine at 7 ns, while in the case of **FM2** the bromine and the coumarin move together and stay at the level of the membrane glycerol group. The bromoalkoxy chain of **FM3** is extended and aligns almost parallel to the lipid acyl chains, as is highlighted by Fig. 4F. In contrast, the **FM2** molecule is strongly tilted with respect to this position (Fig. 4E). The 2*H*-chromen-2-one scaffold in **FM2** is substituted with a more hydrophobic methyl group at C4, and Fig. 4E shows that this methyl group stabilizes an interaction of the coumarin moiety with the hydrophobic portion of the lipids leaving the compound lying parallel to the surface of the membrane. In contrast, the oxygens of the acetyl and 2-ethoxy-2-oxoethyl groups of **FM1** and **FM3** form additional polar interactions with the surface groups of the membrane, with their bromoalkoxy chains more or less parallel to the lipid acyl chains (Fig. 4D and F).

The distributions of the locations of the studied compounds are presented in the histograms of Fig. 5 in terms of the distance of the chromophore center from the center of the bilayer. We applied Gaussian deconvolution to the histograms to assign the most probable values (Table 3). **FM1** can be found with a similar high probability in three preferred locations within the membrane between 9 and 11 Å from the bilayer center (see dots in Fig. 5, and Table 3 for details). In turn, the **FM3** molecule can be found with similar high probabilities at locations 9.30 Å and 11.40 Å from the bilayer center (dots in Fig. 5, and Table 3 for details). A third deeper location with a lesser occurrence was found at 7.62 Å for the latter compound. The narrower distribution of **FM1**, in comparison to **FM3**, indicates that the former has less mobility inside the membrane. Finally, the distribution of **FM2** is shifted toward the membrane surface with only one dominant location at 11.22 Å (Fig. 5 and Table 3), and other locations that are more exposed to the surface (at 11.79 Å and 13.69 Å from the bilayer center), but with less occurrences (Table 3).
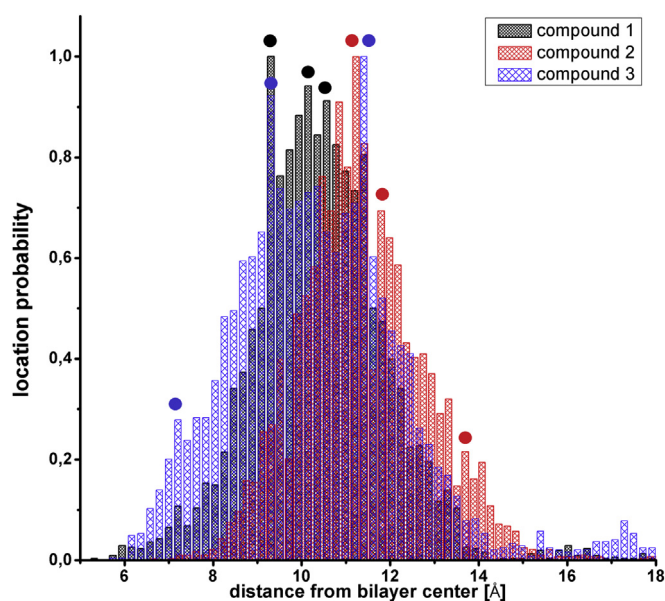

Fig. 5. Location histograms of the chromophore centers of **FM1**, **FM2**, and **FM3** (black, red, and blue plots, respectively) during performed MD simulations. Positions are shown as distance from the bilayer center. Each histogram was normalized by the number of samples indicating the most probable location in a given set of data. Dots correspond to the locations from Table 3. (For interpretation of the references to color in this figure legend, the reader is referred to the web version of this article.)

Table 3

Compound locations in the POPC bilayer obtained by Gaussian deconvolution of data shown in Fig. 3. Distances (in Å) from the bilayer center are reported with calculated normalized amplitudes of peaks (between parentheses).

Compound location (Å)		
FM1	**FM2**	**FM3**
9.30 (1.00)	11.22 (1.00)	11.40 (1.00)
10.14 (0.94)	11.79 (0.69)	9.30 (0.92)
10.56 (0.91)	13.69 (0.21)	7.62 (0.28)

The order parameter S_{CD} of the lipid's acyl chains is defined by the function

$$S_{CD} = <1/2\ 3\ \cos2(\theta_i) - 1>\qquad(1)$$

where θ_i is the instantaneous angle between the *i*th segmental vector of the carbon atoms of the acyl chain and the membrane normal. The calculation is performed for each pose of the MD simulation and averaged over the trajectory ($<\ldots>$ denotes both the ensemble and the time averages). Fig. 4 represents the values of S_{CD} of the pure POPC system as well as the same system when **FM1**−**FM3** are present. As compared to the pure POPC bilayer, the sn-1 and sn-2 chains of the POPC in the systems containing **FM1** or **FM3** show increased order of the chains. However, **FM2** does not affect the order of the POPC sn-1 chain, and shows reduced order at the beginning of the sn-2 chain (Fig. 6).

3. Conclusions

The three coumarin-derived fluorescent probes described here, **FM1**, **FM2** and **FM3**, which localize to the plasma membrane in living cells, have proved useful for labeling this structure in fluorescence microscopy. Molecular dynamics simulations of the insertion of these compounds in a POPC double layer indicate that the substituted coumarin moiety of all three probes interacts with the glycerol moieties near the surface of the membrane. While the bromoalkoxy chains of **FM1** and **FM3** extend to the interior of the membrane, the bromoalkoxy chain of **FM2** lies approximately parallel to the surface. These different orientations suggest the possibility of selectively labeling or otherwise affecting specific regions of a cell membrane using improved probes based on substituted coumarins with long, appropriately functionalized alkyl groups.

4. Experimental

4.1. Materials and instruments

The reagents were purchased from Sigma−Aldrich and were used as received. Unless indicated otherwise, all solutions employed in this study were prepared in HEPES buffer (20 mM; pH 7.4). ^{1}H and ^{13}C NMR spectra were recorded with a Bruker multidimensional 200 MHz spectrometer, using the solvent or the TMS signal as an internal standard. All chemical shifts are reported in the standard δ notation of parts per million. Absorption spectra were recorded at 25 °C using a Perkin Elmer model Lambda 11 spectrometer. Fluorescence spectra were obtained on an Edinburgh Instruments FLS900 fluorescence spectrometer. Data were recorded on-line and analyzed using Origin 8.0 software on a PC. All absorption and emission spectra were measured in a mixture of ACN:aqueous 20 mM HEPES buffer, pH 7.4, 1:1. The X-ray diffraction data were collected using a Bruker SMART platform CCD diffractometer with graphite-monochromatized Mo Kα radiation. The emission spectra were recorded on an ISS PC1 fluorescence

A   POPC: sn-1, 300°K

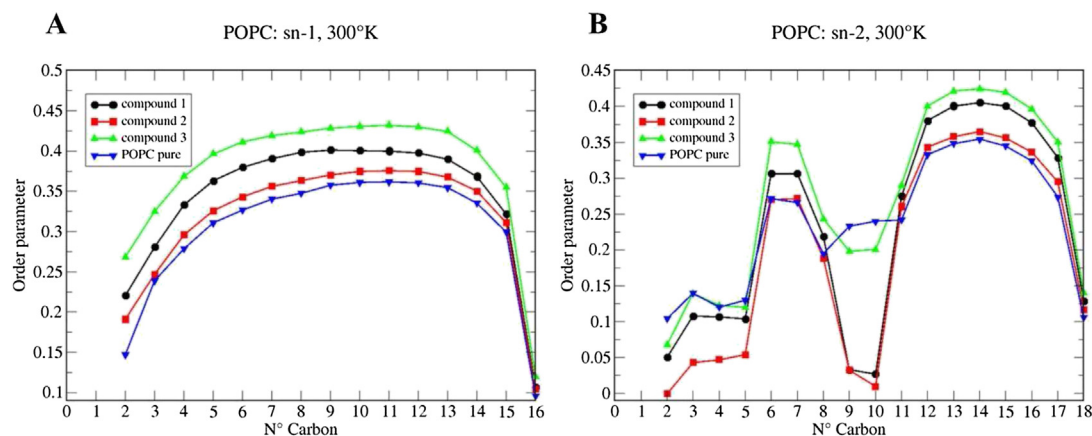**B**   POPC: sn-2, 300°K

Fig. 6. Deuterium order parameters S_{CD} of the (a) sn-1 and (b) sn-2 chains of pure and perturbed POPC systems.

spectrometer. The fluorescence imaging was performed using a Zeiss Hal 100 epifluorescence inverted microscope.

4.2. General synthetic conditions

The coumarin intermediates used in this work were synthesized *via* Pechmann and Knoevenagel condensations to obtain 3-acetyl-7-hydroxy-2-oxo-2*H*-chromene (**2**), 7-hydroxy-2-oxo-2*H*-chromen-4-ylacetic acid (**3**) and ethyl 7-hydroxy-2-oxo-2*H*-chromen-4-ylacetate (**4**) [25,26], which were characterized by ^{1}H and ^{13}C NMR spectroscopy.

4.2.1. 3-Acetyl-7-(6-bromohexyloxy)-2-oxo-2H-chromene (**FM1**)

A mixture of **2** (2.04 g, 0.01 mol), K_2CO_3 (1.38 g, 0.1 mol), and 1,6-dibromohexane (7.32 g, 0.03 mol), was dissolved in DMF (100 mL). The solution was stirred for 4 h at 60 °C and then diluted with water (100 mL). An organic layer that formed was extracted with methylene chloride, and the extract was washed with water, dried, and concentrated to dryness under reduced pressure. The residue was purified by CC using as mobile phase Hex:AcOEt, affording crystals (2.7 g, 70%): mp 116–118. ^{1}H NMR (200 MHz, CDCl₃); δ 8.49 (s, 1H, H-4), 7.54 (d, 1H, *J* = 8.0 Hz), 6.89 (dd, 1H, *J* = 8.0, 1.0 Hz), 6.80 (d, 1H, *J* = 1.0 Hz), 4.06 (t, 3H, *J* = 6.0), 3.44 (t, 3H, *J* = 6.0), 2.70 (s, 3H), 1.89 (m, 4H), 1.53 (m, 4H); ^{13}C NMR (50 MHz, CDCl₃); 195.5, 164.8, 159.8, 157.8, 147.8, 131.5, 120.5, 114.2, 111.9, 100.7, 68.7, 33.7, 32.5, 30.6, 28.7, 27.8, 25.2. *m/z* obsd 389.0364 calcd for $C_{17}H_{19}BrO_4Na$ 388.9995 (Figs. S1A, S1B, S2, Supporting Information).

4.2.2. 7-(6-Bromohexyloxy)-4-methyl-2-oxo-2H-chromene (**FM2**)

A mixture of **3** (2.20 g, 0.01 mol), K_2CO_3 (1.38 g, 0.1 mol) and 1,6-dibromohexane (7.32 g, 0.03 mol), was treated the same as above (yield 2.5 g, 74%): mp 50–52. ^{1}H NMR (200 MHz, CDCl₃) δ 7.48 (d, 1H, Ar–H, *J* = 10.0 Hz), 6.83 (dd, 1H, Ar–H, *J* = 10.0, 2.0 Hz), 6.77 (d, 1H, Ar–H, *J* = 2.0 Hz), 6.10 (s, 1H, H-3), 4.00 (t, 3H, *J* = 6.0), 3.42 (t, 3H, *J* = 6.0), 2.37 (s, 3H, –CH₃), 1.86 (m, 4H), 1.50 (m, 4H), ^{13}C NMR (50 MHz, CDCl₃); δ 162.1, 161.3, 153.3, 152.6, 125.5, 113.5, 112.6, 111.8, 101.3, 68.2, 33.8, 32.6, 28.8, 27.8, 25.1, 18.7. *m/z* obsd 361.0412 calcd for $C_{16}H_{19}BrO_3Na$ 360.9989 (Figs. S3A, S4B, S4; Supporting Information).

4.2.3. Ethyl 7-(6-bromohexyloxy)-2-oxo-2H-chromen-4-ylacetate (**FM3**)

A mixture of **4** (2.48 g, 0.01 mol), K_2CO_3 (1.38 g, 0.1 mol) and 1,6-dibromohexane (7.32 g, 0.03 mol), was treated as above (yield, 2.7 g, 70%): mp 52–54. ^{1}H NMR (200 MHz, CDCl₃); (19.8 g, 83.2%): mp 152–154 °C; ^{1}H NMR (200 MHz, CDCl₃): δ 7.47 (d, 1H, *J* = 8.0),

6.86 (m, 1H), 6.80 (m, 1H), 6.21 (s, 1H, H-3), 4.17 (q, 1H, *J* = 8.0), 4.01 (t, 3H, *J* = 6.0), 3.71 (s, 2H), 3.42 (t, 3H, *J* = 6.0). 1.86 (m, 4H), 1.50 (m, 4H), 1.24 (t, 3H, *J* = 8.0); ^{13}C NMR (50 MHz, CDCl₃); δ 171.5, 162.1, 161.0, 155.5, 152.8, 125.2, 112.7, 111.9, 111.2, 101.8, 68.4, 61.5, 33.8, 32.6, 28.8, 28.4, 27.8, 25.2, 14.0. *m/z* obsd 449.0366 calcd for $C_{19}H_{23}BrO_5K$ 448.9983 (Figs. S5A, S5B, S6; Supporting Information).

4.3. Fluorescence spectroscopy

4.3.1. Calculation of fluorescence quantum yield

Fluorescence quantum yield was determined using quinine sulfate in 0.5 M H_2SO_4 ($\Phi_r = 0.546$) as standard and was calculated using Equation (2) as reported [27],

$$\Phi_s = \Phi_r(A_rF_s/A_sF_r)(\eta_s^2/\eta_r^2) \tag{2}$$

where s and r denote sample and reference, respectively, A is absorbance, F is the relative integrated fluorescence, and η is the refractive index of the solvent.

4.4. X-ray analysis

4.4.1. Refinement

H atoms attached to C4 were located in a Fourier map and their positions and isotropic displacement parameters were refined freely. All other H atoms were positioned geometrically and constrained to ride on their parent atoms (C–H: 0.93–0.97 Å). Displacement factors were taken as $U_{iso}(H) = kU_{eq}(C)$; $k = 1.2–1.5$.

4.4.2. Computing details

Data collection: Bruker *SMART* (BRUKER 1996); cell refinement: Bruker SAINTPLUS V6.02 (BRUKER 1997); data reduction: Bruker *SHELXTL* V6.10 (BRUKER 2000); program used to solve structure: *SHELXS97* (Sheldrick, 1990); program used to refine structure: *SHELXL97* (Sheldrick, 1997) [28,29]. Molecular graphics: *DIAMOND* (Brandenburg, 1999); software used to prepare material for publication: *PLATON* (Spek, 2003) [30,31].

4.5. Cell culture and fluorescence imaging

Human neuroblastoma SH-SY5Y cells (CRL-2266, American Type Culture Collection, Rockville, MD) were cultured in MEM-F12 medium supplemented with 10% FBS, non-essential amino acids, antibiotic–antimycotic mixture, and 20 mM, pH 7.2 HEPES buffer. The medium was replaced every 2 days. Cells were incubated for 20 min with 5 μM **FM1**–**FM3** and 5 μM H. The fluorescence was

observed by epifluorescence microscopy, 63× objective. Red: FM compound, green: H, Yellow: co-localization.

4.6. Molecular modeling of the FM1–FM3 interacting with a lipid membrane

Molecular dynamics (MD) simulations were performed to study the behavior of **FM1**–**FM3** in the vicinity of and within a lipid membrane. MD of the insertion of the studied compounds in the lipid bilayer was modeled using the CHARMM force field [32] in an explicit solvent with the TIP3 water model [33] within the NAMD software [34]. The CGenFF force field [35] was used along with the ParamChem website (https://www.paramchem.org/preview.php) to provide and check the necessary force field parameters for **FM1**– **FM3**. A 1-palmitoyl-2-oleoyl-sn-glycero-3-phosphocholine (POPC) lipid bilayer, composed of 90 lipids (45 per monolayer) and hydrated on each side by 15 Å water slabs, was used as the model. The compounds were immersed in the water medium with the center of mass of each one of them 35 Å from the center of the lipid bilayer. Firstly, each system was minimized (20,000 steps) and equilibrated (5 ns). Then, 50 ns long production MD simulations were performed on each system. During the MD simulations, the equations of motion were integrated with a 2 fs time step in the NPT ensemble. The SHAKE algorithm was applied to all hydrogen atoms; the van der Waals (VDW) cutoff was set to 9 Å. The temperature was maintained at 300 K, employing the Nosé–Hoover thermostat method with a relaxation time of 1 ps. The Nosé–Hoover Langevin piston was used to control the pressure at 1 atm. Long-range electrostatic forces were taken into account by means of the particle-mesh Ewald (PME) approach. Data were collected every 1 ps during the MD runs. Molecular visualization of the systems and MD trajectory analysis were carried out with the VMD software package [36].

Acknowledgments

Appendix A. Supplementary data

Supplementary data related to this article can be found at http://dx.doi.org/10.1016/j.ejmech.2014.02.016.

References

[1] C.W. Cairo, J.A. Key, C.M. Sadek, Fluorescent small-molecule probes of biochemistry at the plasma membrane, Current Opinion in Chemical Biology 14 (2010) 57–63.

[2] A.K. Chamberlain, Y. Lee, S. Kim, J.U. Bowie, Snorkeling preferences foster an amino acid composition bias in transmembrane helices, Journal of Molecular Biology 339 (2004) 471–479.

[3] B. Baird, E.D. Sheets, D. Holowka, How does the plasma membrane participate in cellular signaling by receptors for immunoglobulin E? Biophysical Chemistry 82 (1999) 109–119.

[4] D. English, Z. Welch, A.T. Kovala, K. Harvey, O.V. Volpert, D.N. Brindley, J.G.N. Garcia, Sphingosine 1-phosphate released from platelets during clotting accounts for the potent endothelial cell chemotactic activity of blood serum and provides a novel link between hemostasis and angiogenesis, FASEB Journal 14 (2000) 2255–2265.

[5] F.T. Cooke, Phosphatidylinositol 3,5-bisphosphate: metabolism and function, Archives of Biochemistry and Biophysics 407 (2002) 143–151.

[6] J. Barucha-Kraszewska, S. Kraszewski, P. Jurkiewicz, C. Ranseyer, M. Hof, Numerical studies of the membrane fluorescent dyes dynamics in ground and excited states, Biochimica et Biophysica Acta 1798 (2010) 1724–1734.

[7] S. Oncul, A.S. Klymchenko, O.A. Kucherak, A.P. Demchenko, S. Martin, M. Dontenwill, Y. Arntz, P. Didier, G. Duportail, Y. Mély, Liquid ordered phase in cell membranes evidenced by a hydration-sensitive probe: effects of

[8] U. Ziegler, A. Vinckier, P. Kernen, D. Zeisel, J. Biber, G. Semenza, H. Murer, P. Groscurth, Preparation of basal cell membranes for scanning probe microscopy, FEBS Letters 436 (1998) 179–184.

[9] S.J. Singer, G.L. Nicolson, The fluid mosaic model of the structure of cell membranes, Science 175 (1972) 720–731.

[10] A. Rietveld, K. Simons, The differential miscibility of lipids as the basis for the formation of functional membrane rafts, Biochimica et Biophysica Acta 1376 (1998) 467–479.

[11] D. Brown, J.K. Rose, Sorting of GPI-anchored proteins to glycolipid-enriched membrane subdomains during transport to the apical cell surface, Cell 68 (1992) 533–544.

[12] J.J. Wenz, Predicting the effect of steroids on membrane biophysical properties based on the molecular structure, Biochimica et Biophysica Acta 1818 (2012) 896–906.

[13] E. Blatt, W.H. Sawyer, Depth-dependent fluorescent quenching in micelles and membranes, Biochimica et Biophysica Acta 822 (1985) 43–62.

[14] A. Chattopadhyay, E. London, Parallax method for direct measurement of membrane penetration depth utilizing fluorescence quenching by spin-labeled phospholipids, Biochemistry 26 (1987) 39–45.

[15] F.S. Abrams, A. Chattopadhyay, E. London, Determination of the location of fluorescent probes attached to fatty acids using parallax analysis of fluorescence quenching: effect of carboxyl ionization state and environment on depth, Biochemistry 31 (1992) 5322–5327.

[16] J.R. Silvius, I.R. Nabi, Fluorescence-quenching and resonance energy transfer studies of lipid microdomains in model and biological membranes, Molecular Membrane Biology 23 (2006) 5–16.

[17] L. Bagatolli, To see or not to see: lateral organization of biological membranes and fluorescence microscopy, Biochimica et Biophysica Acta 1758 (2006) 1541–1556.

[18] W. Lesslauer, J.E. Cain, J.K. Blasie, X-Ray diffraction studies of lecithin bimolecular leaflets with incorporated fluorescent probes, Proceedings of the National Academy of Sciences of the United States of America 69 (1972) 1499–1503.

[19] D.A. Cadenhead, B.M.J. Kellner, K. Jacobson, D. Papahadjopoulos, Fluorescent probes in model membranes I: anthroyl fatty acid derivatives in monolayers and liposomes of dipalmitoylphosphatidylcholine, Biochemistry 16 (1977) 5386–5392.

[20] R.D. Klausner, D.E. Wolf, Selectivity of fluorescent lipid analogues for lipid domains, Biochemistry 19 (1980) 6199–6203.

[21] R.G. Ashcroft, K.R. Thulborn, J.R. Smith, H.G.L. Coster, W.H. Sawyer, Perturbations to lipid bilayers by spectroscopic probes as determined by dielectric measurements, Biochimica et Biophysica Acta 602 (1980) 299–308.

[22] L. Loura, F. Fernandes, A.C. Fernandes, J.P. Prates Ramalho, Effects of fluorescent probe NBD-PC on the structure, dynamics and phase transition of DPPC. A molecular dynamics and differential scanning calorimetry study, Biochimica et Biophysica Acta 1778 (2008) 491–501.

[23] W.L. Ash, M.R. Zlomislic, E.O. Oloo, D.P. Tieleman, Computer simulations of membrane proteins, Biochimica et Biophysica Acta 1666 (2004) 158–189.

[24] H.L. Scott, Modeling the lipid component of membranes, Current Opinion in Structural Biology 12 (2002) 495–502.

[25] B. Creaven, D. Egan, K. Kavanagh, M. McCann, A. Noble, B. Thati, M. Walsh, Synthesis, characterization and antimicrobial activity of a series of substituted coumarin-3-carboxylatosilver(I) complexes, Inorganica Chimica Acta 359 (2006) 3976–3984.

[26] A. Manvar, A. Malde, J. Verma, V. Virsodia, A. Mishra, K. Upadhyay, H. Acharya, E. Coutinho, A. Shah, Synthesis, anti-tubercular activity and 3D-QSAR study of coumarin-4-acetic acid benzylidene hydrazides, European Journal of Medicinal Chemistry 43 (2008) 2395–2403.

[27] O. Garcia-Beltrán, N. Mena, E.G. Pérez, B.K. Cassels, M.T. Núñez, F. Werlinger, D. Zabala, M.E. Aliaga, P. Pavez, The development of a fluorescence turn-on sensor for cysteine, glutathione and other biothiols. A kinetic study, Tetrahedron Letters 52 (2011) 6606–6609.

[28] SMART, SAINTPLUS V6.02, SHELXTL V6.10 and SADABS; Bruker Analytical X-ray Instruments Inc., Madison, Wisconsin, USA.

[29] G.M. Sheldrick, SHELXL-97, Program for the Refinement of Crystal Structures, University of Göttingen, Germany, 1997.

[30] K. Brandenburg, DIAMOND, Visual Crystal Structure Information System, in: Version 2.1e Crystal Impact GbR, Bonn, Germany, 1999.

[31] A.L. Spek, Single-crystal structure validation with the program PLATON, Journal of Applied Crystallography 36 (2003) 7–13.

[32] A.D. MacKerell, D. Bashford, M. Bellott, R.L. Dunbrack, J.D. Evanseck, M.J. Field, S. Fischer, J. Gao, H. Guo, S. Ha, D. Joseph-McCarthy, L. Kuchnir, K. Kuczera, F.T.K. Lau, C. Mattos, S. Michnick, T. Ngo, D.T. Nguyen, B. Prodhom, W.E. Reiher, B. Roux, M. Schlenkrich, J.C. Smith, R. Stote, J. Straub, M. Watanabe, J. Wiórkiewicz-Kuczera, D. Yin, M. Karplus, All-Atom empirical potential for molecular modeling and dynamics studies of proteins, Journal of Physical Chemistry B 102 (1998) 3586–3616.

[33] E. Neria, S. Fisher, M. Karplus, Simulation of activation free energies in molecular systems, Journal of Chemical Physics 105 (1996) 1902–1921.

[34] L. Kale, R. Skeel, M. Bhandarkar, R. Brunner, A. Gursoy, N. Krawetz, J. Phillips, A. Shinozaki, K. Varadarajan, K. Schulten, NAMD2: greater scalability for parallel molecular dynamics, Journal of Computational Physics 151 (1999) 283–312.

[35] K. Vanommeslaeghe, E. Hatcher, C. Acharya, S. Kundu, S. Zhong, J. Shim, E. Darian, O. Guvench, P. Lopes, I. Vorobyov, A.D. Mackerell Jr., CHARMM general force field: a force field for drug-like molecules compatible with the CHARMM all-atom additive biological force fields, Journal of Computational Chemistry 31 (2010) 671–690.

[36] W. Humphrey, A. Dalke, K. Schulten, VMD: visual molecular dynamics, Journal of Molecular Graphics 14 (1996) 33–38.

[37] W. Meldenson, S. Hayden, Preparation of 2,4-dihydroxybenzaldehyde by the Vilsmeier-Haack reaction, Synthetic Communications 26 (1996) 603–610.

[38] Y. Oshiro, S. Sato, N. Kurahashi, T. Tanaka, T. Kikuchi, K. Tottori, Y. Uwahodo, T. Nishi, Novel antipsychotic agents with dopamine autoreceptor agonist properties: synthesis and pharmacology of 7-[4-(4-phenyl-1-piperazinyl) butoxy]-3,4-dihydro-2(1H)-quinolinone derivatives, Journal of Medicinal Chemistry 41 (1998) 658–667.

[39] F. Jafarpour, N. Jalalimanesh, M.B. Amiri Olia, A.O. Kashani, Silver-catalyzed facile decarboxylation of coumarin-3-carboxylic acids, Tetrahedron 66 (2010) 9508–9511.

[40] R. Grainger, A. Nikmal, J. Cornella, I. Larrosa, Selective deuteration of (hetero) aromatic compounds via deutero-decarboxylation of carboxylic acids, Bioorganic & Medicinal Chemistry 10 (2012) 3172–3174.

[41] Z. Wang, L. Zhu, F. Yin, Z. Su, Z. Li, C. Li, Silver-Catalyzed decarboxylative C chlorination of aliphatic carboxylic Acids, Journal of the American Chemical Society 134 (2012) 4258–4263.

[42] J. Cornella, C. Sanchez, D. Banawa, I. Larrosa, Silver-catalyzed protodecarboxylation of carboxylic acids, Chemical Communications 45 (2009) 7176–7178.

[43] H.-Z. Zhang, Q.-X. Li, B.-T. Yin, C.-H. Zhou, 7-(6-Bromohexyloxy)-4-methyl-2H-chromen-2-one, Acta Crystallographica E68 (2012) o1709.

[44] K. Sivakumar, F. Jesurethinam, K. Subramanian, S. Natarajan, 7-Hydroxy-4-coumarinacetic acid monohydrate, Acta Crystallographica Section C: Crystal Structure Communications C46 (1990) 1663–1665.

[45] A. Galdámez, O. García-Beltrán, B.K. Cassels, Hydrogen-bonded supramolecular array in the crystal structure of ethyl 7-hydroxy-2-oxo-2H-chromene-3-

[46] C.-L. Xu, N. Yang, G.-Y. Yang, S.-F. Fan, C.-Y. Niu, Cinnamyl 2-oxo-2H-chromene-3-carboxylate, Acta Crystallographica E65 (2009) o2991.

[47] Y.-Y. Zhang, Y. Shi, C.-H. Zhou, 4-Methyl-7-[2-(1H-1,2,4-triazol-1-yl)-ethoxy]-2H-chromen-2-one, Acta Crystallographica E67 (2011) o892.

[48] J. Bernstein, R.E. Davis, L. Shimoni, N.-L. Chang, Patterns in hydrogen bonding: functionality and graph set analysis in crystals, Angewandte Chemie International Edition in English 34 (1995) 1555–1573.

[49] G.R. Desiraju, The C-H···O hydrogen bond in crystals: what is it? Accounts of Chemical Research 24 (1991) 290–296.

[50] G.R. Desiraju, The C-H···O hydrogen bond: structural implications and supramolecular design, Accounts of Chemical Research 29 (1996) 441–449.

[51] R.M. Silverstein, G.C. Bassler, T.C. Morrill, Spectrometric Identification of Organic Compounds, fifth ed., Wiley, Singapore, 1991.

[52] T.A. Moore, M.L. Harter, P.S. Song, Ultraviolet spectra of coumarins and psoralens, Journal of Molecular Spectroscopy 40 (1971) 144–157.

[53] C. Karapire, H. Kolancilar, Ü. Oyman, S. Icli, Fluorescence emission studies with 6- and 5,6-benzocoumarins and a 5,6-benzochrome, Journal of Photochemistry and Photobiology A 153 (2002) 173–184.

[54] K. Muthuramu, V. Ramamurthy, 7-Alkoxy coumarins as fluorescence probes for microenvironments, Journal of Photochemistry 26 (1984) 57–64.

[55] J.R. Heldt, J. Heldt, M. Stoń, H.A. Diehl, Photophysical properties of 4-alkyl- and 7-alkoxycoumarin derivatives. Absorption and emission spectra, fluorescence quantum yield and decay time, Spectrochimica Acta A 51 (1995) 1549–1563.

[56] T. Baumgart, G. Hunt, E.R. Farkas, W.W. Webb, G.W. Feigenson, Fluorescence probe partitioning between Lo/Ld phases in lipid membrane, Biochimica et Biophysica Acta 1768 (2007) 2182–2194.

[57] J.E. González, R.Y. Tsien, Improved indicators of cell membrane potential that use fluorescence resonance energy transfer, Chemistry & Biology 4 (1997) 269–277.

[58] J. Barucha-Kraszewska, S. Kraszewski, P. Jurkiewicz, Ch. Ramseyer, M. Hof, Numerical studies of the membrane fluorescent dye dynamics in ground and excited states, Biochimica et Biophysica Acta 1798 (2010) 1724–1734.